Appl Phys A (2009) 95: 1079–1088
DOI 10.1007/s00339-009-5114-5

Applied Physics A
Materials Science & Processing

Integrated receiver architectures for board-to-board free-space optical interconnects

Feiyang Wu · Logeeswaran VJ · M. Saif Islam · David A. Horsley · Robert G. Walmsley · Sagi Mathai · Denny Houng · Michael R.T. Tan · Shih-Yuan Wang

Received: 14 September 2008 / Accepted: 16 December 2008 / Published online: 19 February 2009

Abstract In many computer and server communications copper cables and wires are currently being used for data transmission and interconnects. However, due to significant shortcomings, such as long transmission time, high noise level, unstable electrical properties, and high power consumption for cooling, researchers are increasingly turning their research interests toward alternatives, such as fiber optic interconnects and free-space optical communication technologies. In this paper, we present design considerations for an integrated receiver for high-speed free-space line-of-sight optical interconnects for distortion-free data transmission in an environment with mechanical vibrations and air turbulences. The receiver consists of an array of high-speed photodiodes for data communication and an array of quadrant photodiodes for real-time beam tracking in order to compensate for the beam misalignment caused by vibrations in servers. Different configurations for spatially positioning the quadrant and data photodiodes are discussed for 4×4 and 9×9 multielement optical detector arrays. We also introduce a new beam tracking device, termed the strip quadrant photodiodes, in order to accurately track highly focused optical beams with very small beam diameter.

F. Wu · L. VJ · M.S. Islam (✉)
Department of Electrical and Computer Engineering,
University of California at Davis, Davis, CA 95616, USA
e-mail: saif@ece.ucdavis.edu
Fax: +1-530-7528428

D.A. Horsley
Department of Mechanical and Aeronautical Engineering,
University of California at Davis, Davis, CA 95616, USA

R.G. Walmsley · S. Mathai · D. Houng · M.R.T. Tan · S.-Y. Wang
Information and Quantum Systems Lab, Advanced Studies,
Hewlett-Packard Laboratories, Palo Alto, CA 94304, USA

PACS 07.07.Tw · 42.30.Tz · 85.60.Gz · 85.60.-q · 85.60.Dw

1 Introduction

Over the past two decades, the Internet experienced an explosive growth from the advent of numerous network applications such as peer-to-peer (P2P) file sharing, voice communications, and video over IP. At present, healthcare, financial, communication, and entertainment industries rely heavily on Internet-based computing and data processing. By some estimates, the amount of data being processed is doubling every year, leading to a projection for a 1000-fold increase in ten years [1]. Almost the entire structure of the Internet is based upon a client–server model which is chiefly designed around board-to-board connections via copper cables. However, these copper cables are becoming the bottleneck in improving the speed and power efficiency of the computers and data servers [2]. The speed of a server connection needs to keep up with increasing Internet traffic demand at data transmission rates of 10 Gbps or even higher at 100 Gbps [2]. The current copper cables are limited by speed and size, which is a direct result of parasitic resistance, capacitance, and inductance. At low frequencies, the series resistance and shunt capacitance of a circuit board copper trace dominate the communication behavior determining the transition times and thereby limiting the data transmission rate. At higher frequencies, the wire's series inductance becomes more dominant than the resistance as an impeding factor contributing to the same end result—a limit on the rate at which the trace can transmit signal pulses. All these parasitic factors depend heavily on the geometry of the wire, especially the physical length. Resistance, for instance, is proportional to the wire's length

and inversely proportional to its cross-sectional area. Because of this dependence on geometry, a simple wire's ultimate bitrate turns out to be proportional to its cross section, but falls with the square of its length. So, thinner and especially longer cables results in a lower data transfer bitrate. Transition-time limitations can be addressed by several alternatives that are unfortunately not compatible with noise minimization, power requirements, and thermal management [3]. The heat generated by the cables requires more than 50% of the total energy consumed by the cooling devices [4]. If the data transfer rate is increased, the heat generated by the cables occupies a larger percentage of the cooling power and significantly contributes to lowering the system efficiency.

Free-space optical (FSO) interconnects have the potential to boost data throughput between computers and servers by a factor of 1000 because of the high data rate of optics and the fact that optical data channels can be more densely packed than their electrical counterpart [2]. As a consequent, FSO interconnects; combined with electronics, offer a potential solution to ease the communication bottleneck of interconnects. Alignment between the optical transmitter and receiver is the key factor that establishes the viability and the performance of the optical link. Innovative techniques are thus needed to assemble optical components in a rugged yet simple way that is fully compatible with conventional electronic packages while reducing their manufacturing and operating cost. A great deal of research has been conducted on line-of-sight FSO communication for long distances such as inter-satellite links as well as short distances such as inter-building communications that span distances up to a few kilometers [5–8]. Several groups have also worked on shorter links for applications in computer servers. Esener et al. [9] have reported extensive studies using hybrid one-dimensional arrays of devices to demonstrate free-space optical interconnect on printed circuit boards for computer interconnects [9–11]. Previous efforts have mainly focused on understanding the core issues of atmospheric turbulence, beam misalignment, and error corrections [8, 12, 13], while very minimal work was done on developing the low-cost advanced detector arrays for high-speed FOS links.

In this paper, we present the design considerations and system simulations of an integrated receiver for inter-server communications with high-speed FOS interconnects in an environment with incessant mechanical vibrations and air turbulences from internal and external sources.

2 Receiver design with integrated quadrant photodiodes (QPDs)

Figure 1 illustrates the general concept of integrated FOS links that can be used for server-to-server crosslinks. Electrical signals, from server 'A' modulate a set of parallel laser beams generated by vertical-cavity surface-emitting lasers (VCSELs). Relative vibration between the two servers causes the received laser beam (data) to wander over the detection plane contributing to degradation of system performance due to the beam spot moving out of the detection area and causing random fluctuations of the signal intensity at the receiver. As a solution, a pair of MEMS devices integrated with a pair of lenses is integrated to the server processing boards for real-time optical beam alignment.

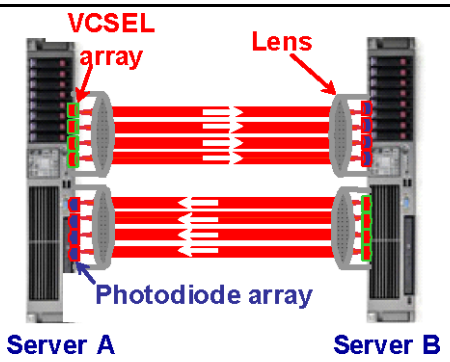

Fig. 1 Board-to-board optical interconnect networks. The data beams originate from server 'A' and traverse through the free space between the lenses and are detected by an array of photodiodes placed at the board of server 'B'. An identical process exchanges data between the VCSEL's of server 'B' and the photodiode array of server 'A'

The data beams traverse through the free space between the lenses and are detected by an array of photodiodes positioned at the board of server 'B'. An identical process exchanges data between the VCSELs of server 'B' and the photodiode array of server 'A'. This scheme of communication is based on three major components: (a) an array of lasers (VCSELs), (b) MEMS devices for beam aligning (control/tracking), and (c) an integrated receiver array with slow photodetectors for beam tracking (quadrant photodiodes) and a set of high-speed photodetectors for data communication. This paper will focus on the design of a low-cost integrated receiver that can be integrated with MEMS devices for real-time beam tracking in order to compensate for the beam misalignment caused by relative vibration of the servers. Our proposed solution is based on monolithic integration of quadrant photodiodes (QPDs—a four-element array) for beam positioning and high-speed data photodiodes (DPDs) for information processing.

Our beam tracking QPD design is based on a widely used mechanism in conventional optical data storage technology including CD and DVD devices [14]. A misaligned beam incident on a QPD induces a voltage representing the tracking error. The tracking devices are then activated to scan and search initially on horizontal then vertical directions, in order to stay locked and in focus. Between two servers, several tens to hundreds of channels are expected to communicate through the free space in the form of linear or square arrays

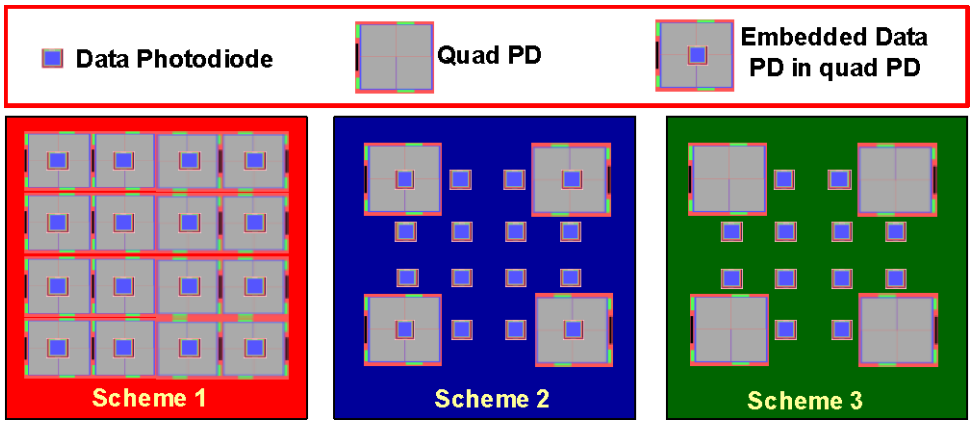

Fig. 2 Three different schemes for arranging a 4 × 4 square array of photodiodes. In our work, data photodiodes (DPDs) have a size of 50 μm × 50 μm, Quad photodiodes (QPD) have a size of 300 μm × 300 μm and the beam spot is ∼40–50 μm in diameter. Scheme 1 contains 16 QPD with DPDs, Scheme 2 contains four QPDs with DPDs embedded in them at four corners, and 12 stand-alone DPDs and Scheme 3 contains four QPDs, and 12 single DPDs

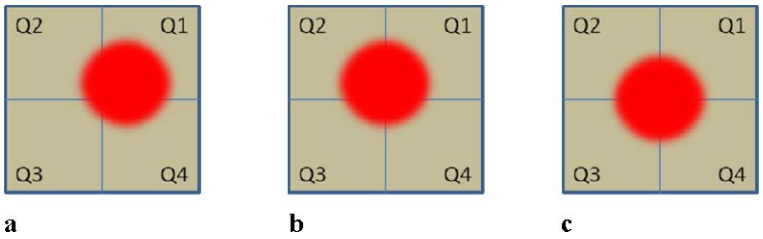

Fig. 3 (**a**) Initial beam position located on a QPD, with readout Q1: 60%, Q2: 15%, Q3: 15%, Q4: 10%. The QPD readout indicates that beam center is located on Q1, thus it should move to the left until the readout of Q1 + Q4 is equal to that of Q2 + Q3. (**b**) Subsequent to the horizontal adjustment, the readout ratios are Q1:Q2:Q3:Q4 = 35%:35%:15%:15%. Since Q1 + Q2 > Q3 + Q4, it needs to be moved downward, until the readout of all four elements are equalized. (**c**) Final beam position, with Q1 = Q2 = Q3 = Q4 = 25%

such as 4 × 4 and 9 × 9 arrays. Figure 2 depicts three possible integration methods under consideration:

1. Scheme 1: DPDs are embedded at the center of QPDs.
2. Scheme 2: QPDs are only at four corners with embedded DPDs.
3. Scheme 3: QPDs are at four corners and the rest of the positions of the array are DPDs.

Scheme 1 has the advantage of monitoring the positions of all of the data channels separately and offers considerable redundancy. Considering the fact that a large number of channels is required between two servers, deploying a pair of quadrant and data photodiodes for each channel would be prohibitively costly making it an unattractive option. Scheme 2 has one QPD with embedded DPDs at each corner of the array. A QPD in one corner monitors the position while it is counterpart in another corner monitors angular misalignment. An additional redundant pair of quadrant photodiodes is used for monitoring two active quadrant photodiodes. Although this scheme is more attractive compared to Scheme 1, its drawback is the low accuracy of the position monitoring which is limited by the size of the data photodiode at the center, which is 50 μm × 50 μm in our case for demonstration purposes.

Scheme 3 is similar to Scheme 2, except for the four corners that are solely QPDs instead of embedded DPDs. This design increases the accuracy of the beam position monitoring by taking out the DPD from the QPD in each corner of the array (4 × 4 array in this case). Better accuracy in the beam positioning places the beam at the center of the DPDs contributing to higher efficiency in the light absorption. In the subsequent discussion, we will focus on Scheme 3 for designing our receiver array.

Individual elements in QPDs produce a current that is proportional to the light intensity falling on it. A voltage readout is obtained by a current-to-voltage converter and an amplifier. In a FSO link, the QPD would detect data beam misalignment by sensing different voltage readouts in the four quadrants. A higher voltage readout in one of the elements of a QPD that indicates a beam misalignment and triggers a beam alignment process by steering the beam in both vertical and horizontal directions until all the QPD elements sense identical voltage readouts. The MEMS, devices for beam aligning, then locks the beams at the exact center of the photodiodes.

An example of the QPD-based alignment mechanism is shown in Fig. 3. In Fig. 3a, most of the beam spot is located in Q1. Consequently, the voltage readout, which is proportional to the power absorbed in each element of a quadrant photodiode, is ∼60% in Q1, 15% in Q2, 15% in Q4, and 10% in Q3. In order to align the beam back to the center, the beam will be horizontally steered to the left until the voltage

readout of left quadrants (Q2 + Q3) equals that of the right quadrants (Q1 + Q4), as shown in Fig. 3b. This aligns the beam to the horizontal center and a final beam movement would bring the beam back to the vertical center by sensing and comparing the voltages readouts of the top quadrants (Q1 + Q2) with that of the bottom quadrants (Q3 + Q4). When the voltage readouts of all the elements are equal, i.e., Q1 = Q2 = Q3 = Q4, the beam is exactly aligned.

Angular misalignment can be addressed by using two QPDs in an array as shown in Scheme 3 on Fig. 2. When the elements of two different QPDs have different readouts, it is an indication of an angular misalignment and the MEMS devices go through rotational beam alignment before triggering a translational alignment.

3 Receiver design with strip quadrant photodiodes (SQPDs)

We now introduce a new design for position sensing with high spatial resolution and data stream tracking with a very small beam spot. The device is constructed by dividing standard QPDs along the two diagonals and further segmenting them into thinner strips as shown in Fig. 4. The device, termed strip quadrant photodiodes (SQPDs), is capable of beam tracking with high precision for a large misalignment limited by the size of the quadrant photodiodes.

In the SQPDs, upon illumination, a small beam spot can be detected at the exact region where it is incident on, and the system can use that information to align the beam back to the center. A precise alignment method can be implemented by a maximum of two step beam alignment process. The design in Fig. 4c can be further modified by separating it into four sections, and positioning each section around a 9 × 9 data photodiodes array as shown in Fig. 5.

We describe the alignment procedure and present some simulation examples of misaligned beams to develop the alignment algorithm of the beam with SQPDs. For naming convention, we assign T, B, L, and R, as shown in Fig. 5a, to each strip in a SQPD and assign 1 to 4 for each strip, starting from shortest to longest, as shown in Fig. 5b. We also assume that each strip is 40 μm wide and the beam spot size is 50 μm in diameter.

We set a decision rule to determine whether a beam is considered located on the strip or in between two strips, so that the largest misalignment is 10 μm. The rule is illustrated by the following calculation:

For a beam spot with Gaussian distribution profile, the power $P(r, z)$ passing through a circle of radius r in the transverse plane at position z can be written as:

$$P(r, z) = P_0\left(1 - e^{\frac{-2r^2}{w(z)^2}}\right) \tag{1}$$

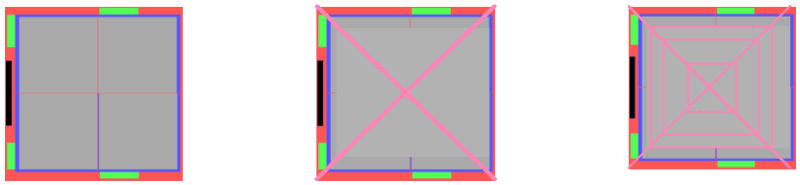

a **b** **c**

Fig. 4 Sequence of designing SQPD from a standard square QPD. (**a**) Current square quad photodiode is divided in four equal segments via lateral and vertical divisions. (**b**) Devices with similar effectiveness can be designed by dividing them through the diagonals resulting in four regions: *top*, *bottom*, *left* and *right*. (**c**) A highly precise beam tracking mechanism is developed by dividing the QPD of (**b**) into four strips resulting in a SQPD with sixteen segments

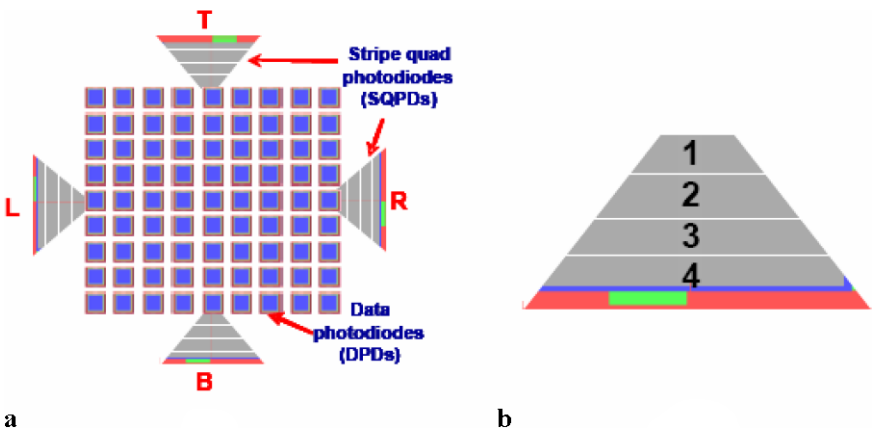

a **b**

Fig. 5 (**a**) Photodiodes array (9 × 9) with SQPDs. A QPD is segmented into four sections, and positioning around a DPD array. A total of 16 segments of the SQPD are essential for the beam alignment process. (**b**) Naming convention for the example calculation for the alignment algorithm

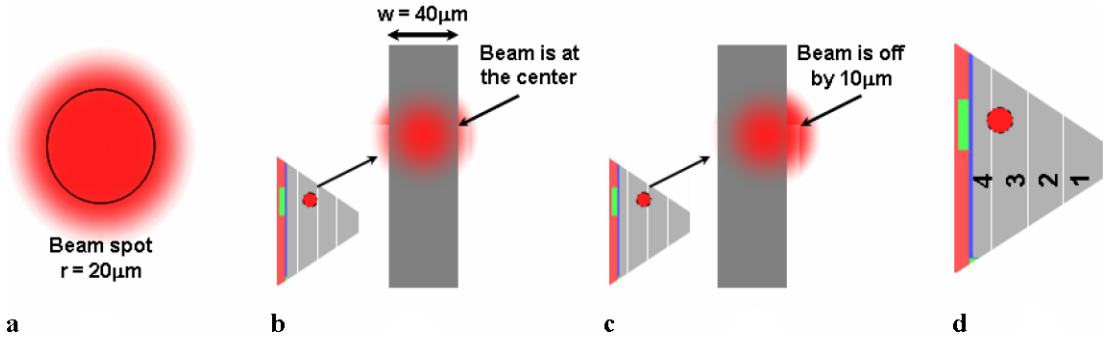

Fig. 6 Device parameters used in developing alignment algorithm. (**a**) Beam spot incident on the detector array is ∼40 μm. (**b**) Each strip in the SQPDs is 40 μm wide. The *circle* with a diameter of 40 μm represents the beam spot, which is located at the strip center when perfectly aligned, and located 10 μm off the center of the strip for a particular case of misalignment. (**c**) By calculating the fraction of optical power outside a strip and comparing the total beam power, we develop an algorithm for aligning the beams with better than 10 μm accuracy. (**d**) A beam located mostly on strip 3 and with very little overlap with strip 4 can be approximated as located in strip 3 with ∼10 μm misalignment

where $w(z)$ is the diameter of the beam at distance z and P_o is the total energy. In our devices, we estimate our $w(z)$ to be ∼20 μm. Therefore, the fraction of beam power detected by the SQPDs over total beam power is:

$$F = \frac{P(r)}{P_0} = 1 - e^{-0.005r^2} \tag{2}$$

In order to calculate the boundary conditions for Gaussian beam profile, for case b from Fig. 6d, where the beam is 10 μm away from the strip center, we decompose $P(r)$ into $P(x, y)$ where $x^2 + y^2 = r^2$ and integrate to find the total incident power on the SQPDs. While it is almost 100% for good beam alignment (Fig. 6b), it is about 84% for the case shown in Fig. 6c. Our algorithm is based on the calculation as follows. When 84% or more of optical energy is detected on one single strip, we consider the data beam spot to be at the center of that strip of the SQPD. If one of the strips of the SQPDs detects less than 84% of the incident beam, the beam is located between two strips and alignment algorithm takes this into consideration.

The rule is applied to the following example, where each strip is 40 μm wide, and the DPD is 50 μm × 50 μm. In Fig. 6d, let us consider the total incident optical power on the L strip of the SQPD is 100 μW. (L1 + L2 + L3 + L4 = 100 μW), and L3 absorbs ∼88 μW. We can conclude that the beam spot is located at the center of L3, as a result, in order for the beam to be adjusted for accurate alignment, it has to go through half of the strip L3 width and the entire width of strip L1 and L2. In other words, the total beam displacement is the addition of the width of strip L1 and L2, plus half of the width of strip L3 and half of the width of the DPD (which is a total displacement of 20 μm + 40 μm + 40 μm + 25 μm = 125 μm in our example). Similarly, total displacement for vertical alignment can be calculated based on the voltage readings of the top and bottom SQPDs.

Based on the rule mentioned previously, we calculated the total beam tracking requirements along with possible residual misalignment in the beams. Using a data photodiode with a dimension of 50 μm × 50 μm and SQPD with a strip width of 40 μm, we can have a maximum misalignment of 15 μm if the lower limit of the SQPDs is set to 84% of the incident beam power. Table 1 presents some calculations on this alignment scheme. The first column shows the location of the beam, second column shows the direction of the beam movement for alignment, and the fourth column shows the total possible misalignment in the data beams. The SQPDs can similarly be used for estimating the angular misalignment of the data beam.

Typical VCSELs exhibit a doughnut-shaped beam profile with a non-Gaussian power distribution and hence the proposed beam tracking and alignment mechanism for the Gaussian beam can be modified. The following method can be adapted to generate a table for calculating the beam misalignment for any arbitrarily varying VCSEL beam shape.

1. Monitor a strip (such as L3 as shown Fig. 6), scan the VCSEL beam slowly to maximize the power on L3 (measured power is P1).
2. Control the VCSELs to move the beam 10 μm to the right (measured power is P2).
3. Divide P2 by P1, the resultant fraction could be used in defining misalignment and generating a table.

These adjustment rules would handle the translational misalignment. Angular misalignment can be addressed by an additional alignment step. Subsequent to the adjustment of the translational misalignment, the optical power of all four DPDs adjacent to the each quarter of SQPD can be monitored. Any disparity in the four readings would be an indication for angular misalignment.

Table 1 Misaligned beams are located in the first column and the direction of the beam alignment is shown in the second column

Beam position in the SQPDs	Direction of beam alignment	Total beam movement (μm)	Max possible misalignment (μm)
T1	Down	40	15
T1/2	Down	65	14
T2	Down	90	13
T2/3	Down	115	12
T3	Down	140	13
T3/4	Down	160	13
T4	Down	180	11
B1	Up	40	15
B1/2	Up	65	14
B2	Up	90	13
B2/3	Up	115	12
B3	Up	140	13
B3/4	Up	160	13
B4	Up	180	11
L1	Right	40	15
L1/2	Right	65	14
L2	Right	90	13
L2/3	Right	115	12
L3	Right	140	13
L3/4	Right	160	13
L4	Right	180	11
R1	Left	40	15
R1/2	Left	65	14
R2	Left	90	13
R2/3	Left	115	12
R3	Left	140	13
R3/4	Left	160	13
R4	Left	180	11

4 Design comparison

In this section, we compare the advantages and disadvantages for both the QPDs and SQPDs considering some extreme operating case scenarios. The QPDs are able to detect the position of the beam in terms of which quadrant it is located, as indicated by the voltage readout. However, the ability of detecting the magnitude of beam misalignment, such as, how far away it is from the center or which exact location it is on the quadrant, depends on the spot size. For example, Fig. 7 shows a small beam spot located at the second quadrant inducing a voltage readout. Two circumstances are considered here: in case *a*, the beam spot is located in the second quadrant, near the left end close to the horizontal axis. In case *b*, the beam spot is again located in the second quadrant, but it is near the top end and close to the vertical axis. Even though both positions are at two extreme locations of the second quadrant, we cannot apply the same beam tracking algorithm to align the beam of the photodiode since their exact locations are different. However, the voltage readings from the QPDs, the only information we get from the receiver, suggests that the misalignment is identical in nature (contrary to the reality, as shown in Fig. 7, the voltage of the left two quadrants minus the right two quadrants, V_{L-R} and voltage of the bottom two quadrants minus the top two quadrants, V_{B-T} are both 3 and -3 V, respectively in these two cases). Designing smaller QPDs could be a possible solution but that will contribute to a higher risk of unrealizable complex beam tracking.

Concept of SQPD reduces QPD footprints and makes each data photodiode in the array available for communication. The advantages of SQPDs are more accurate sensing of distance and direction of the misalignment, along with only two steps for position adjustment and accurate alignment of the beam, in particular, when the spot size is small. On the other hand, a QPD shown in Fig. 4a will require at least four times larger spot size for sensing and relocating the position of the beam. Moreover, at least two QPDs will

be needed for the alignment process (as shown in Fig. 2) contrary to the need for only one SQPD in this scheme. The angular misalignment can also be corrected using a single SQPD. In addition, the number of steps for relocating the beam would always be exactly two for SQPDs—one horizontal and one vertical movement. The number of steps, however, is unpredictable for a QPD due to the fact that it has to go through a length scan-and-search mechanism. On the other hand, because the relocation algorithm is based on a precalculated table, the SQPD cannot achieve as high spatial accuracy as that of QPD. The maximum misalignment between the final beam center and the center of a photodiode is 15 μm in our example. Whether a FSO will be able to tolerate this misalignment will depend on the system requirements, beam profile, data transmission rate, and size of the active devices. It is clear that QPDs offer more advantages for locking the beam to the center of the photodetectors with high accuracy at the cost of lengthy scan-and-search mechanism.

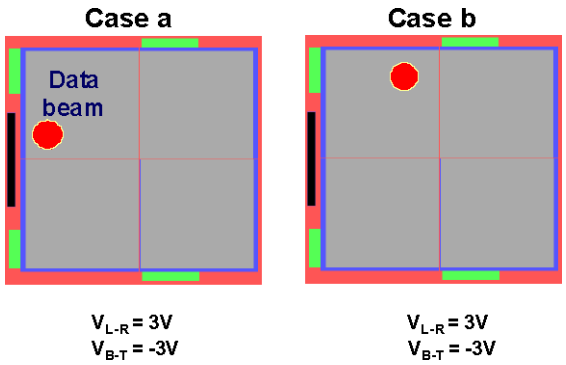

Fig. 7 Issues with accurate beam tracking using QPDs. In general, two outputs for QPD are produced to determine the exact location of a laser beam, V_{L-R} and V_{B-T}. V_{L-R} represents the voltage of the left two quadrants minus the right two quadrants, and V_{B-T} represents the voltage of the bottom two quadrants minus the top two quadrants. The combination of these two outputs would decide the location of the spot. The special cases shown here illustrate that for some small beam spot, the usual outputs of QPDs do not provide enough information to determine the exact location. Here both case *a* and *b* show the data beam to be in the same QPD, but are not misaligned with identical characteristics

5 Simulation details and results

In this section, we describe the detailed simulation that we performed for the two designs we discussed in this paper and analyze their respective impact on the overall system. For the simulation of beam alignment mechanism using both SQPDs and QPDs, 100 points are randomly generated with initial positions designated with coordinates (x_0, y_0), where x_0 and y_0 vary between a margin of ± 150 μm. Each point is considered as the initial position of the Gaussian beam spot. In general, both SQPD and QPD methods have their distinctive ways of monitoring and recording the initial beam positions, and track the beam to compensate for the misalignment. The simulation records the number of steps to move each beam to a final aligned position at the center of the DPD. For both simulation methods, we assume that the beam has the Gaussian profile with a radius of 20 μm and the SQPD and QPD have a total size of 300 μm × 300 μm.

SQPD simulation method Our simulation strategy is to generate some random positions of beam centers and correlate them to the SQPD power reading. We first define coordinates for each strip in an SQPD. For example, Fig. 8 shows segment 1 and 2 of strip R (as shown in Fig. 5), where R1 and R2 are defined by the range: $0 < x < 40$ and

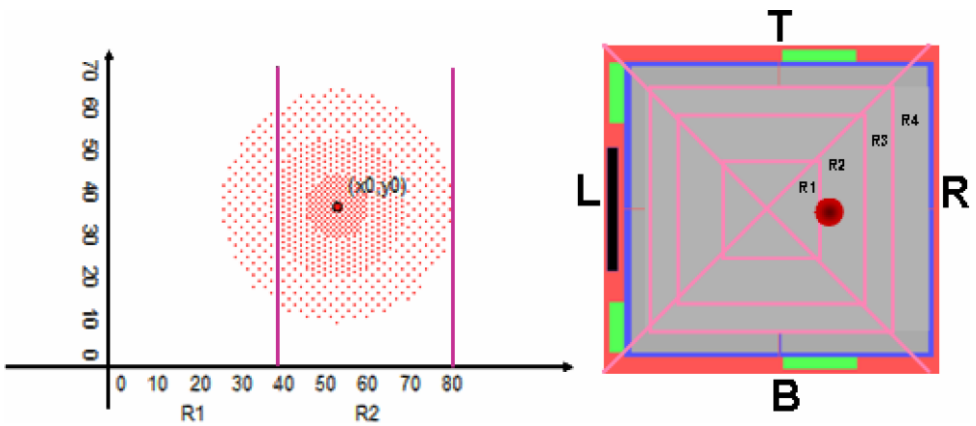

Fig. 8 Correlation between the initial beam positions and SQPD readings. Initial beam center position is (x_0, y_0). The beam is represented by a *circle* with radius of 20 μm around (x_0, y_0) and it contains 100 dots with a distribution similar to a Gaussian beam profile (lower concentration of *dots* at the edge of the *circle*). By counting number of points inside each SQPD region (R1 and R2 in this figure), a correlation with the absorbed power in the SQPD can be made. A *red spot* on the SQPD (*right figure*) shows the position of the beam

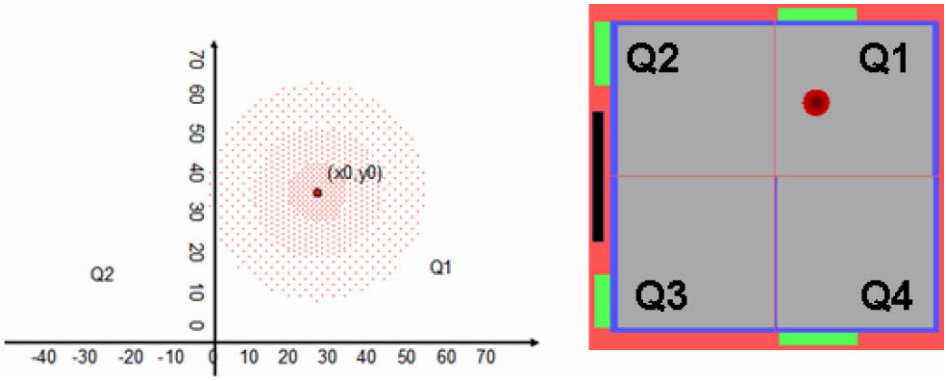

Fig. 9 Correlation between the initial beam positions and QPD readings. Initial beam center position is (x_0, y_0). The beam is represented by a *circle* with radius of 20 μm around (x_0, y_0) and it contains 100 dots with a distribution similar to a Gaussian beam profile (lower concentration of dots at the edge of the circle). By counting number of points inside each QPD region (Q1 and Q2 in this figure), a correlation with the absorbed power in the QPD can be made. A *red spot* on the QPD (*right figure*) shows the position of the beam

$40 < x < 80$, respectively. The beam is represented by a circularly shaped Gaussian beam of radius 20 μm. The beam is represented by dots, each symbolizing a unit of optical power and is spatially positioned to maintain a concentration gradient that resembles a Gaussian beam profile (high concentration of power at the center). By counting the number of dots on each strip, the fraction of incident beam power is estimated. For example in Fig. 8, 90% of the dots are located in R2. Therefore R2 absorbs 90% of the beam power. This piece of information is used in determining the precise location of the beam and a table similar to Table 1 is used to determine the direction and magnitude of the beam movement. This technique allows us to align the beam in two steps using SQPD.

QPD simulation method We used a similar method as described in the previous section for SQPD-based beam alignment. Here we move the beam in steps of 5 μm in lateral direction until the power reading on both Q1 and Q2 are identical. Similar vertical and subsequently horizontal beam movement help in positioning the beam at the center of the QPD. The total number of movement is the sum of the steps in both vertical and horizontal direction.

Figure 10a shows that a SQPD aligns a misaligned beam in only two steps for any random location. On the other hand, a QPD requires a larger number of steps for beam alignment, with a mean of 18.25 steps and a large standard deviation of 6.38 steps. However, there is a trade-off between number of steps for beam alignment and the residual misalignment. Although SQPD allows a faster alignment of a misoriented beam in only two steps, it could result in an average misalignment of ∼8 μm, greater than that of a system built with QPD, which is 5.6 μm as shown in Fig. 10b. The standard deviation of residual misalignment of SQPD is 4.42 μm, which is also greater than that of QPD (0.73 μm).

A comparison of average power absorption in data photodiodes (DPDs) in free-space links based on QPD and SQPD does not show a discernable difference. Simulation results presented in Fig. 10c shows ∼76% average absorption in the DPDs for a link with QPD and ∼75% average absorption for a link build with SQPDs—a mere 1% difference between the average powers. Although these values are very close, the absorption in DPDs in a link based on SQPD has four times larger standard deviation (∼8%) than that of QPDs (∼2%). The minimum absorption in the DPDs is ∼67% for a SQPD-based link (acceptable range of power absorption) and it can go as high as 100% ideally. On the other hand, the QPD counterpart offers a DPD absorption between 70% to 80%. All these results indicate that SQPD is preferable for a stable system performance, although there is a trade-off between ease of alignment and residual misalignment.

6 Conclusion

We presented an integrated receiver design for high-speed free-space optical interconnects for data transmission between two servers and/or computers. Different configurations for the multielement receiver arrays that consist of high-speed data photodiodes and beam tracking quadrant photodiodes (QPDs) are discussed. A new beam tracking mechanism, termed strip quadrant photodiode (SQPDs), is developed for accurate beam tracking when the beam spot is very small. Related calculations, assumptions and algorithms for beam tracking are provided. Simulations of links with QPD- and SQPD-based alignment mechanisms are presented and a SQPD-based link is found to be more robust. The devices may contribute to a rack-to-rack, board-to-board, and eventually chip-to-chip interconnects making free-space optical links an engineering reality with acceptable cost-to-performance ratio. This detection mechanism

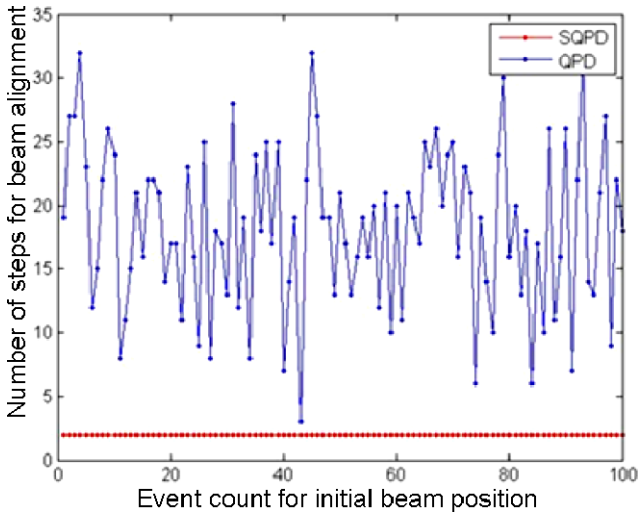

a

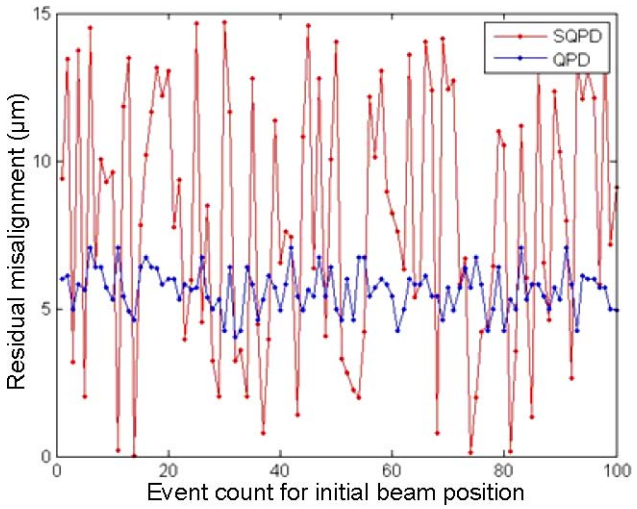

b

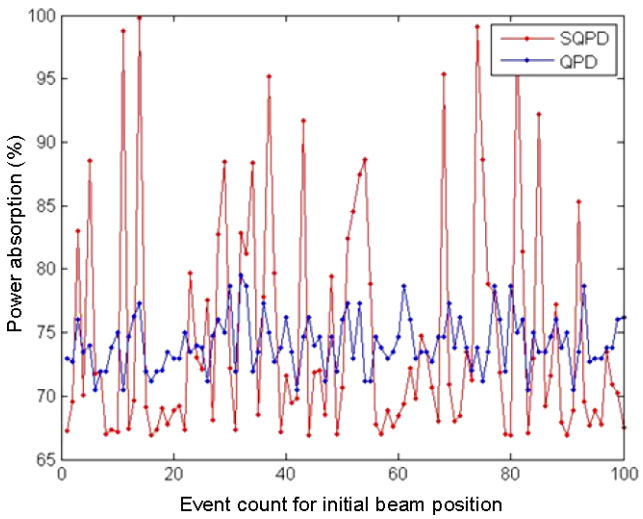

c

◀ **Fig. 10** (**a**) Number of steps vs. event counts for initial beam position. X-axis represents a total of 100 events. For each initial beam position, SQPD and QPD are used to align the beam to the center position. The number of steps for SQPD and QPD to align the beam are recorded and plotted. The Y-axis corresponds to that number of steps. The simulation suggests that irrespective of the initial beam position, it takes two steps for aligning using a SQPD, but the steps for aligning using a QPD varies from 3 to 33 steps. (**b**) Residual misalignment vs. event counts for initial beam position. For each initial beam position, SQPD and QPD are used to align the beam to the center position. The distance between the final beam position and the origin are plotted in the Y-axis for both SQPD and QPD based alignment methods. The results suggest that QPD will align a beam with an average of 5 μm misalignment. SQPD, on the other hand, will have a misalignment ranging between 0 to 15 μm. (**c**) Power absorption (%) vs. Event count for initial beam position. For each initial beam position, SQPD and QPD are used to align the beam to the center position. Subsequently, the power absorption for a square shaped data photodiode with a size of 50 μm × 50 μm is calculated. The figure suggests that QPDs result in consistent power absorption of ∼75%; ranging between 70% to 80%; whereas a link with SQPDs demonstrates power absorption between 67% to 100% in the data photodiodes. A quantum efficiency of 100% is assumed in this simulation

can be applied not only in free-space optical interconnects for beam tracking, but also in enhancing the performance of vision-based real-time tracking systems as well as automated robotic systems.

Acknowledgement The work at UC Davis was supported by Hewlett-Packard Company and National Science Foundation (CAREER Grant #0547679).

References

1. L. Roberts, Packet networks, presented at the SIGCOMM'99, Boston, MA, Aug. 1999
2. N. Savage, Linking with light. IEEE Spectrum **39**(8), 32–36 (2002)
3. D.A. Gilliland, Server cooling and exhaust appendage system. US 2007/0190920 A1, Feb 15, 2006
4. S.W. Montgomery, W. Berry, M. Engineer, High-density architecture meets electrical and thermal challenges. Intel Developer Update Magazine (2002)
5. M. Gerken, G. Luichtel, Free-space, laser-based data transmission: satellite communication as a technology driver for the development of fast, reliable terrestrial data networks. Proc. SPIE **6975**, 697508 (2008)
6. V.W.S. Chan, Optical satellite networks. J. Lightw. Technol. **21**(11), 2811–2827 (2003)
7. X. Zhu, J.M. Kahn, Free-space optical communication through atmospheric turbulence channels. IEEE Trans. Commun. **50**(8), 1293–1300 (2002)
8. N. Cvijetic, S.G. Wilson, R. Zarubica, Performance evaluation of a novel converged architecture for digital-video transmission over optical wireless channels. IEEE/OSA J. Lightw. Technol. **25**(11), 3366–3373 (2007)

9. G.I. Yayla, P.J. Marchand, S.C. Esener, Speed and energy analysis of digital interconnections: comparison of on-chip, off-chip, and free-space technologies. Appl. Opt. **37**, 205–227 (1998)
10. X.Z. Zheng, P.J. Marchand, D.W. Huang et al., Optomechanical design and characterization of a printed-circuit-board-based free-space optical interconnect package. Appl. Opt. **38**(26), 5631–5640 (1999)
11. W.H. Wu, L.A. Bergman, A.R. Johnston, C.C. Guest, S.C. Esener, P.K.L. Yu, M.R. Feldman, S.H. Lee, Implementation of optical interconnections for VLSI. IEEE Trans. Electron. Dev. **34**, 706–714 (1987)
12. J.A. Anguita, I.B. Djordjevic, M.A. Neifeld, B.V. Vasic, Shannon capacities and error-correction codes for optical atmospheric turbulent channels. OSA J. Opt. Netw. **4**(9), 586–601 (2005)
13. M. Uysal, J. Li, M. Yu, Error rate performance analysis of coded free-space optical links over gamma-gamma atmospheric turbulence channels. IEEE Trans. Wirel. Commun. **5**(6), 1229–1233 (2006)
14. M. Mansuripur, G. Sincerbox, Principles and techniques of optical data storage. Proc. IEEE **85**(11), 1780–1796 (1997)